NEW SYNCHRONIZATION METHOD FOR THREE-PHASE THREE-WIRE PWM CONVERTERS UNDER UNBALANCED AND DISTORTED GRID VOLTAGES

Robinson F. de Camargo and Humberto Pinheiro
Universidade Federal de Santa Maria
Grupo de Eletrônica de Potência e Controle
CEP 97105-900, Santa Maria – RS – Brasil
e-mail: robinsonfcamargo@hotmail.com humberto@ctlab.ufsm.br

***Abstract* –This paper proposes a new *open-loop* synchronization method for three-phase three-wire PWM converters connected to the utility grid. It presents a good performance under unbalanced and highly distorted grid voltages. Moreover, it has a better performance in terms of distortions in the synchronization signals if compared with other *open-loop* methods and it has a good transient performance due amplitude, frequency and angle disturbances. In addition, a frequency adaptation algorithm is proposed for applications where large frequency variations are expected, such as in weak grids. Experimental results using a DSP TMS320F2812 are given to demonstrate the good performance of the proposed synchronization method.**

***Keywords* - New Synchronization Method, Normalized Voltage, Positive Sequence, Three-Phase Three-Wire PWM Converters.**

I. INTRODUCTION

Several techniques to synchronize PWM converters to the utility grid have been reported. They can be classified as *closed-loop* [1-5, 21, 24-26] and *open-loop* [6-13, 23] methods. In *closed-loop* methods the angle of synchronization is obtained through a *closed-loop* structure, which aims at locking the estimated value of the phase angle to its actual value. On the other hand, *open-loop* synchronization methods, the synchronization angle or normalized synchronization vector is obtained directly from the grid voltages [6, 7, 9], virtual flux [8, 10, 11] or estimate grid voltages [12, 13].

Although *closed-loop* methods have low sensitivity to the grid frequency, a trade off between good transient response and good filtering characteristics must always be considered. Moreover, the phenomenon of cycle slips is usually present in *PLL closed-loop* methods. When these methods are used to synchronize PWM converters to grid, this phenomenon can result in large transient currents during the resynchronization [20].

Among *open-loop* methods, the modified synchronous reference frame (*MSRF*) [6, 7] and the low-pass filter based (*LPF-B*) methods [9] standout for their simplicity. The main attribute of the former is to be independent of the grid frequency. The latter, the space vector filter (*SVF* and *MSVF*) [9] and the extended Kalman filter (*EKF*) [5] are less sensitive to grid harmonics. Moreover, the weighted least-squares estimation (*WLSE*) [17] rejects the impact of negative-sequence and accommodates frequency variations. However, none of *open-loop* methods reported so far, have a good performance in terms of the distortion in synchronization signals under unbalance and harmonics in the grid voltages.

In this sense, this paper proposes a new *open-loop* synchronization method for three-phase three-wire PWM converters connected to the utility grid that provides a good performance in terms of synchronization signals, even in the presence of harmonics and severe unbalance among grid voltages. Experimental results demonstrate the good performance of the proposed method using a DSP TMS320F2812 controller.

Manuscript received on May 14, 2005; first revision on August 30, 2005; second revision on September 20, 2005. Recommended by the Editor of the Special Section Edson H. Watanabe.

II. PROPOSED SYNCHRONIZATION METHOD

The proposed synchronization method is called normalized positive sequence synchronous frame, *NPSF*, and it is shown in the Fig. 1 for three-phase three-wire systems. It can be applied to three-phase four-wire system with small modifications [27], as well. From the measure of two line-to-line grid voltages, the normalized positive sequence synchronization vector in the fundamental frequency is obtained.

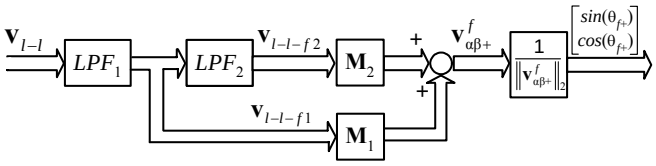

Fig. 1. Proposed normalized positive sequence reference frame for three-phase three-wire systems.

As usually the PWM converters are analyzed and controlled considering phase quantities [18, 19], the line-to-line voltages vector, $v_{l\text{-}l}$, is transformed into a phase voltage vector, v_{ph}. This transformation is not unique, so, it will be assumed that the sum of the phase voltages is zero. Then:

$$\mathbf{v}_{ph} = \mathbf{T}_{l-ph}\mathbf{v}_{l-l}, \tag{1}$$

where:

$$\mathbf{v}_{ph} = \begin{bmatrix} v_a \\ v_b \\ v_c \end{bmatrix} \quad \mathbf{T}_{l-ph} = \frac{1}{3}\begin{bmatrix} 2 & 1 \\ -1 & 1 \\ -1 & -2 \end{bmatrix} \quad \mathbf{v}_{l-l} = \begin{bmatrix} v_{ab} \\ v_{bc} \end{bmatrix}. \tag{2}$$

Now, by considering that the grid voltages usually have some degree of unbalance, depending on the synchronization

method used, this disturbance generates distortion in synchronization signals [2, 17]. In order to avoid this distortion, the synchronization vector will be generated from the positive sequence components of the grid voltages at the fundamental frequency.

Fortescue in his theory of symmetrical components applied to phasor quantities proposed the following complex matrix to extract the positive sequence component

$$\frac{1}{3}\begin{bmatrix} 1 & a & a^2 \\ a^2 & 1 & a \\ a & a^2 & 1 \end{bmatrix} = \begin{bmatrix} 1/3 & -1/6 & -1/6 \\ -1/6 & 1/3 & -1/6 \\ -1/6 & -1/6 & 1/3 \end{bmatrix} + \begin{bmatrix} 0 & 1/6 & -1/6 \\ -1/6 & 0 & 1/6 \\ 1/6 & -1/6 & 0 \end{bmatrix} j \cdot \quad (3)$$

The operator a rotates a phasor by 120º while j rotates 90º. Note that this concept can be extended to the time domain, in the following to:

$$\mathbf{v}_{ph+}^{f} = \mathbf{T}_{+\_R}\mathbf{v}_{ph}^{f} + \mathbf{T}_{+\_I}S_{90}\left(\mathbf{v}_{ph}^{f}\right), \quad (4)$$

where the T_{+R} e T_{+I} are the real matrices at the right side of the (4) and the $S_{90}(\cdot)$ is an operator that implements 90º phase-shift at the fundamental in the frequency in the time domain. This operator implementation will be addressed in the next subsection. The vectors in (4) are given by:

$$\mathbf{v}_{ph+}^{f} = \begin{bmatrix} v_{a+}^{f} \\ v_{b+}^{f} \\ v_{c+}^{f} \end{bmatrix}, \mathbf{v}_{ph}^{f} = \begin{bmatrix} v_{a}^{f} \\ v_{b}^{f} \\ v_{c}^{f} \end{bmatrix}, \quad (5)$$

In (5), the superscript f and subscript + represent the fundamental frequency and the positive sequence, respectively.

A simple way to obtain the synchronization vector is by transforming grid voltages into αβ stationary coordinates [6, 7]. Here, in the same way, the positive sequence phase voltages at the fundamental frequency will be transformed to αβ coordinates, that is,

$$\mathbf{v}_{\alpha\beta+}^{f} = \mathbf{T}_{\alpha\beta}\mathbf{v}_{ph+}^{f}, \quad (6)$$

where:

$$\mathbf{v}_{\alpha\beta+}^{f} = \begin{bmatrix} v_{\alpha+}^{f} \\ v_{\beta+}^{f} \end{bmatrix}, \mathbf{T}_{\alpha\beta} = \sqrt{\frac{2}{3}}\begin{bmatrix} 1 & -1/2 & -1/2 \\ 0 & \sqrt{3}/2 & -\sqrt{3}/2 \end{bmatrix}, \quad (7)$$

To simplify the transformations presented in (1), (4) and (6), they can be combined as follows:

$$\mathbf{v}_{\alpha\beta+}^{f} = \mathbf{T}_{\alpha\beta}\mathbf{T}_{+\_R}\mathbf{T}_{l\text{-}ph}\mathbf{v}_{l-l}^{f} + \mathbf{T}_{\alpha\beta}\mathbf{T}_{+\_I}S_{90}\left(\mathbf{T}_{l\text{-}ph}\mathbf{v}_{l-l}^{f}\right), \quad (8)$$

which can also be expressed as:

$$\mathbf{v}_{\alpha\beta+}^{f} = \mathbf{M}_2\left(-\mathbf{v}_{l-l}^{f}\right) + \mathbf{M}_1 S_{90}\left(\mathbf{v}_{l-l}^{f}\right), \quad (9)$$

where:

$$\mathbf{M}_1 = \frac{1}{2}\begin{bmatrix} 0 & -\sqrt{2}/2 \\ \sqrt{6}/3 & \sqrt{6}/6 \end{bmatrix}, \mathbf{M}_2 = \frac{1}{2}\begin{bmatrix} -\sqrt{6}/3 & -\sqrt{6}/6 \\ 0 & -\sqrt{2}/2 \end{bmatrix}. \quad (10)$$

Note that $v_{\alpha\beta}{}^{f}{}_{+}$ is the grid positive sequence phase voltage vector at the fundamental frequency in αβ coordinates. Thus, its amplitude depends on the grid voltage. A normalized synchronization vector can be obtained dividing $v_{\alpha\beta}{}^{f}{}_{+}$ by its norm, that is,

$$\mathbf{v}_{\alpha\beta+n}^{f} = \frac{\mathbf{v}_{\alpha\beta+}^{f}}{\left\|\mathbf{v}_{\alpha\beta+}^{f}\right\|_2}, \quad (11)$$

where this Euclidian norm of the vector is given by:

$$\left\|\mathbf{v}_{\alpha\beta+}^{f}\right\|_2 = \sqrt{\left(v_{\alpha+}^{f}\right)^2 + \left(v_{\beta+}^{f}\right)^2}. \quad (12)$$

The entries of the vector $v_{\alpha\beta}{}^{f}{}_{+n}$ (11) can be understood as being the sine and cosine often used to synchronize PWM converters with the grid, that is,

$$sin\left(\theta_{f+}\right) = v_{\beta+n}^{f} \text{ and } cos\left(\theta_{f+}\right) = v_{\alpha+n}^{f}, \quad (13)$$

where $\theta_{f+}=\omega_f t$ and ω_f is the grid fundamental frequency.

In order to obtain $v_{\alpha\beta}{}^{f}{}_{+n}$, it is required to find $S_{90}\left(\mathbf{v}_{l-l}^{f}\right)$ and $-\mathbf{v}_{l-l}^{f}$. The next section describes how these quantities are obtained in the time domain.

Implementation of the Phase-Shifter S_{90} in Time Domain

In [2], the phase-shifter S_{90} has been implemented in the time domain with all-pass filters, which are designed to provide unit gain and 90º phase-shift at the fundamental frequency. However, this approach does not consider the harmonics in the grid voltages, which corrupt the synchronization signals [2, 5].

As an alternative, this paper considers the use of low-pass filters to reduce the harmonics present in v_{l-l} as well as to implement the 90º phase-shift at the fundamental frequency as required to compute the positive sequence.

Firstly, the v_{l-l} vector is firstly filtered using a low-pass filter, LPF_1, which generates a filtered vector, v_{l-l-f1}. This vector has its fundamental voltage -90º shifted from the fundamental of v_{l-l}. The v_{l-l-f1} vector is filtered again using another low-pass filter, LPF_2. This provides an additional -90º phase-shift, resulting in the filtered vector v_{l-l-f2}, which presents the same amplitude at the fundamental of the original vector v_{l-l}, but with -180º phase-shift.

Thus, the output of the LPF_1 filter will be $S_{90}\left(\mathbf{v}_{l-l}^{f}\right)$ and the LPF_2 output will be $-\mathbf{v}_{l-l}^{f}$, which are required to compute $\mathbf{v}_{\alpha\beta+}^{f}$.

The low-pass filters LPF_1 and LPF_2 are designed in a similar way. The second order transfer function of the implemented filters in the s domain is:

$$G(s) = \frac{\omega_n^2}{s^2 + 2\zeta\omega_n s + \omega_n^2}, \quad (14)$$

Note that the parameters of the filter must be selected so that:

$$G(s)\big|_{s=j\omega_f} = 1\angle -90°, \quad (15)$$

where, $\omega=2\pi f$ rad/s. To satisfy this condition, $\omega_n = 2\pi f$ and $\zeta=0.5$.

In the discrete domain, the low-pass filters may be implemented by the following discrete state space equation:

$$\begin{aligned} x(k+1) &= \mathbf{G}x(k) + \mathbf{H}u(k) \\ y(k) &= \mathbf{C}x(k) \end{aligned}, \quad (16)$$

The equation (16) has been obtained by the discretization of (14), using a zero order hold (ZOH) with a sampling period T_s. The frequency response of the LPF filter implemented with (16) is shown in Fig. 2. It can be seen that at 60 Hz, the filter presents a unit gain and a -90º phase-shift. In addition, voltage harmonics are significantly reduced; for instance at the output of LPF_1 the 3rd is attenuated 19 dB and the 5th, 28

dB. At the output of LPF_2 the 3rd is attenuated 38 dB and the 5th, 56 dB.

Note that the -90º phase-shift occurs at 60Hz. In cases where the grid frequency varies significantly, the filter parameters must be updated. On the other hand, it sub-harmonics is a concern, it is possible to add a band-pass filtes with unit gain and zero-degree phase-shift at the fundamental frequency to avoid undesired distortions.

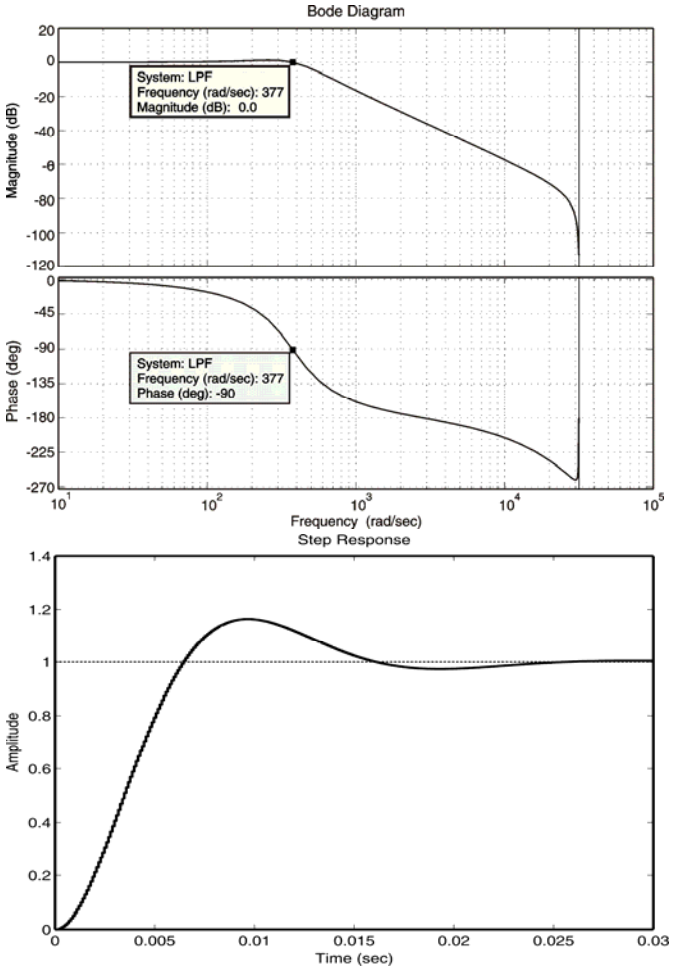

Fig. 2. Bode diagram of the LPF_1 or LPF_2 and step response.

The next section proposes an adaptation algorithm for the filter parameters.

III. FREQUENCY ADAPTATION ALGORITHM

In stiff grids, the frequency variations in the algorithm to be considered is not a concern, since the utility companies usually provide a grid voltage with frequency regulated between ± 1 Hz, as recommended by IEC 61000-2-2.

However, in isolated or emergency energy systems [22], the frequency variations can exceed the limits mentioned above. So, to broaden the range of applications of the synchronization method to weak grid, a frequency adaptation algorithm is proposed. Its block diagram adds to the *NPSF* method is shown in Fig. 3.

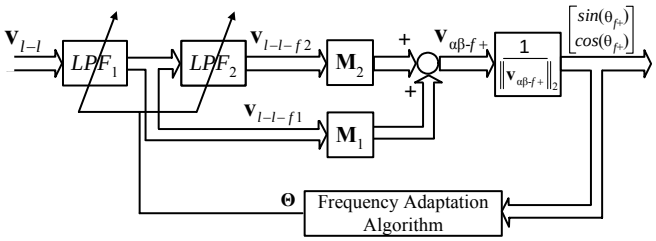

Fig. 3. Proposed normalized positive sequence reference frame for three-phase three-wire systems with frequency adaptation algorithm.

Details of the frequency adaptation algorithm are given in Fig. 4. It consists of a low-pass filter, LPF_3, identical to LPF_1 and LPF_2. The LPF_3 filters the normalized synchronization vector obtained, (11), and from the result its square norm is calculated that is,

$$\left\| \mathbf{v}_{sc-f} \right\|_2^2, \tag{17}$$

If the natural frequency of the filter ω_n is to equal the grid frequency, then (17) results in 1. However, if $\|v_{sc-f}\|_2^2>1$ this indicates that the natural frequency of the filter ω_n is bigger than the grid frequency. On the other hand, if $\|v_{sc-f}\|_2^2<1$, this indicates that ω_n is smaller than the fundamental frequency of the grid. Then, the error, $1-\|\mathbf{v}_{sc-f}\|_2^2$ can be used to estimate the grid frequency, $\hat{\omega}$, using an integrator, as shown in Fig. 4. Therefore, using the $\hat{\omega}$, the matrices **G**, **H** and **C** of the low-pass filters can be updated. In Fig. 4, the parameter set $\mathbf{\Theta}$ represents the union of the filter matrices, that is, $\mathbf{\Theta} = \mathbf{G} \cup \mathbf{H} \cup \mathbf{C}$.

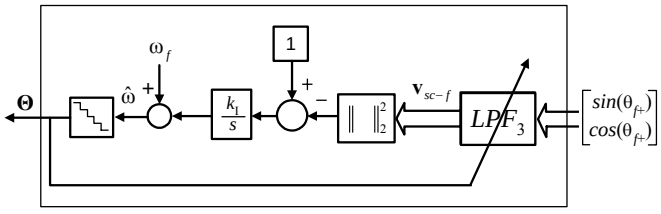

Fig. 4. Proposed frequency adaptation algorithm.

Frequency Adaptation Algorithm Gain Design

First to design the gain of the frequency adaptation algorithm, a nonlinear model will be developed. The block diagram of the nonlinear model of this adaptation algorithm is shown in Fig. 5, where the dynamics of LPF_3 have not been considered to simplify the controller design. In sinusoidal steady-state, the relationship between $\|\mathbf{v}_{sc-f}\|_2^2$, the grid frequency and the estimated frequency can be expressed as follows:

$$f\left(\hat{\omega},\omega\right) = \left\| \mathbf{v}_{sc-f} \right\|_2^2 = \frac{1}{\left[1-\left(\frac{\omega}{\hat{\omega}}\right)^2\right]^2 + \left(\frac{\omega}{\hat{\omega}}\right)^2} \tag{18}$$

By linearizing the system shown in Fig. 5 around the nominal operation point, a linear model is obtained as shown in Fig. 6. This model will be used in the design of the integrator gain.

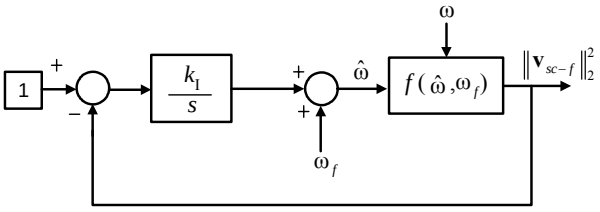

Fig. 5. Block diagram of the nonlinear model.

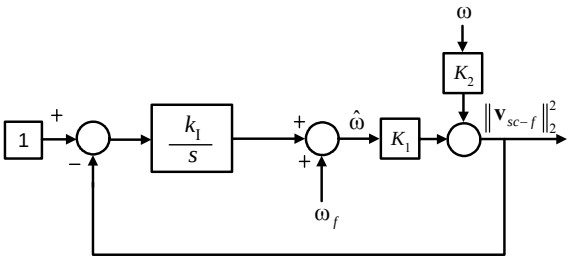

Fig. 6. Block diagram of the linearized model.

The parameters K_1 and K_2 are:

$$K_1 = \frac{\partial f}{\partial \hat{\omega}}\bigg|_{\hat{\omega}=\omega_f,\omega=\omega_f}, \tag{19}$$

$$K_2 = \frac{\partial f}{\partial \omega}\bigg|_{\hat{\omega}=\omega_f,\omega=\omega_f}. \tag{20}$$

Thus, substituting (18) in (19) and (20) the parameters K_1 and K_2 are obtained, which are:

$$K_1 = -K_2 = \frac{2}{\omega_f}. \tag{21}$$

Finally, defining the bandwidth of frequency adaptation algorithm as B_ω, the integrator gain can be obtained as follows:

$$k_1 = \frac{B_\omega}{K_1} = \frac{B_\omega \omega_f}{2}. \tag{22}$$

where, ω_f is the grid nominal frequency.

As an example, if the bandwidth of the adaptation algorithm is equal to one tenth the grid frequency, that is, $B_\omega = (1/10)\omega_f$, then $k_1 \cong 7{,}106$.

Therefore, the frequency estimation algorithm can be summarized as:

$$\hat{\omega} = \omega_f + \frac{k_I}{s}\left(1 - \left\|\mathbf{v}_{sc-f}\right\|_2^2\right). \tag{23}$$

In cases where there is grid frequency variation, the low-pass filters parameters are updated. The proposed algorithm transient behavior due to frequency variations is presented in the experimental section.

IV. EXPERIMENTAL RESULTS

This section demonstrates the performance of the proposed method through experimental results considering four conditions for the utility grid: a) Grid voltages balanced without distortions; b) Grid voltages unbalanced without distortions; c) Grid voltages balanced with distortions and d) Grid voltages unbalanced with distortions.

The proposed synchronization method has been implemented in a TMS320F2812 DSP controller with fixed-point arithmetic. The execution time of the synchronization algorithm took 6.5 μs of the CPU time, allowing rising up the sampling frequency to 40 kHz.

A. Grid Voltages Balanced without Distortions

Fig. 7 shows the experimental results of the v_{ab} (top) and v_{bc} (bottom) line-to-line grid voltages in p.u. are under $THD_v \cong 0\%$ and $UF_v \cong 0\%$. The total harmonic distortion (THD_v) and unbalanced factor (UF_v) are defined in the Appendix. Fig. 8 presents the *sine* (top) and *cosine* (bottom) generated by the *NPSF* method under this condition.

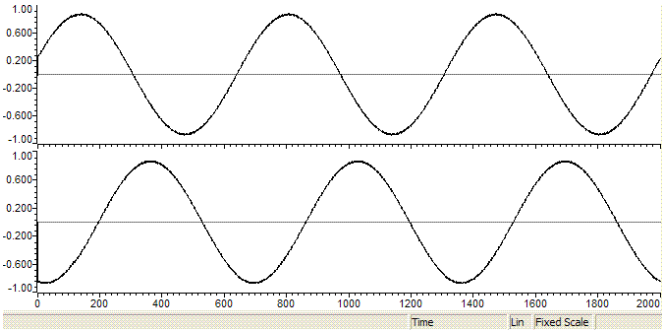

Fig. 7. Line-to-line grid voltages with $THD_v \cong 0$ % and $UF_v \cong 0\%$. Horizontal scale: sample, Ts=25μs. Vertical scale: v_{ab} and v_{bc} in p.u.

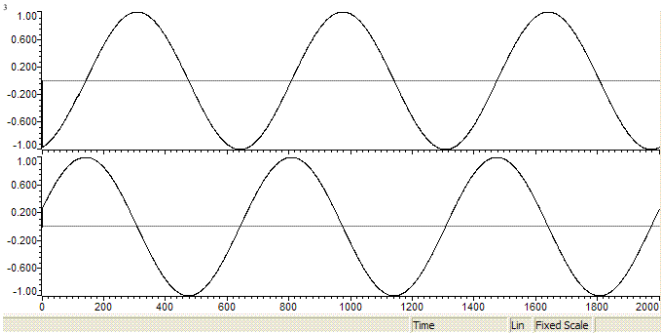

Fig. 8. Synchronization signals obtained using the *NPSF* method for the voltages of Fig. 7. Horizontal scale: sample, Ts=25μs. Vertical scale: *sine* and *cosine*.

B. Grid Voltage Unbalanced without Distortions

In this case the THD_v is kept close to zero but the unbalance factor is to 68% as shown in the Fig. 9. Fig. 10 presents the *sine* (top) and *cosine* (bottom), where, is possible to see that the synchronization signals do not present a significant distortion. These demonstrate the good performance of the proposed method to obtain the positive sequence.

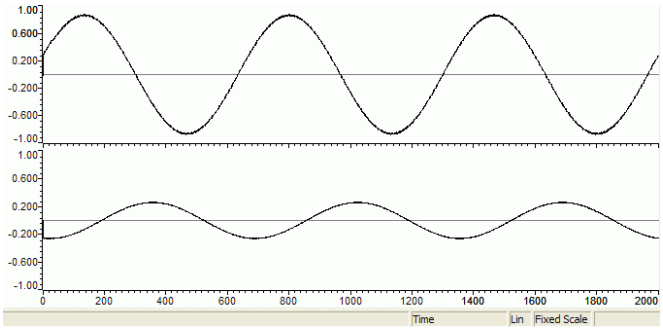

Fig. 9. Line-to-line grid voltages with THD_v≅0 % and UF_v=68%. Horizontal scale: sample, Ts=25µs. Vertical scale: v_{ab} (top) and v_{bc} (bottom) in p.u.

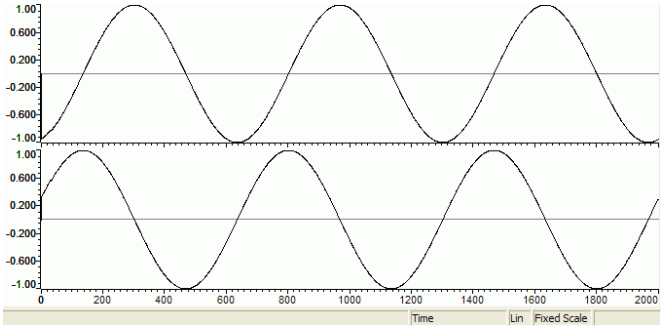

Fig. 10. Synchronization signals obtained using the *NPSF* method with the voltages of Fig. 9. Horizontal scale: sample, Ts=25µs. Vertical scale: *sine* (top) and *cosine* (bottom).

C. Grid Voltage Balanced with Distortions

This case considers that the line-to-line voltages are distorted by 5ª, 7ª, 11ª, 13ª, 17ª harmonic components. This harmonics results in THD_v=7.5 % and UF_v≅0 % as shown in Fig. 11. Fig. 12 presents the *sine* (top) and *cosine* (bottom), where, is possible to see that the synchronization signals do not present a significant distortion. This is mainly due to the low-pass filters (LPF_1 and LPF_2).

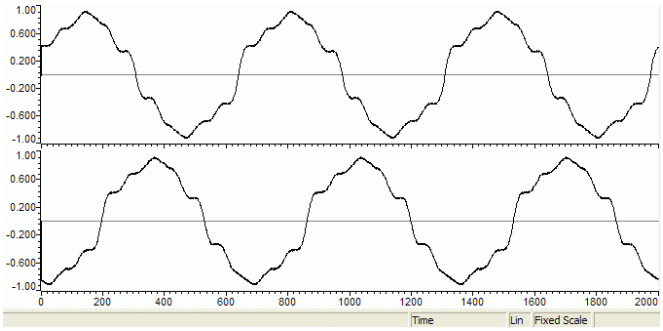

Fig. 11. Line-to-line grid voltages under THD_v=7.5 % and UF_v≅0%. Horizontal scale: sample, Ts=25µs. Vertical scale: v_{ab} and v_{bc} in p.u.

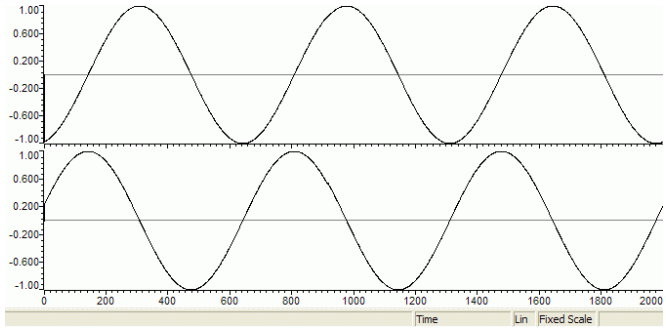

Fig. 12. Synchronization signals obtained using the *NPSF* method consider the voltages of Fig. 11. Horizontal scale: sample, Ts=25µs. Vertical scale: *sine* and *cosine*.

D. Grid Voltage Unbalanced with Distortions

Fig. 13 presents experimental results where line-to-line grid voltages have a THD_v=7.5 % and with an UF_v=68 %. Again, the *sine* (top) and *cosine* (bottom) shown in the Fig. 14 do not present a significant distortion.

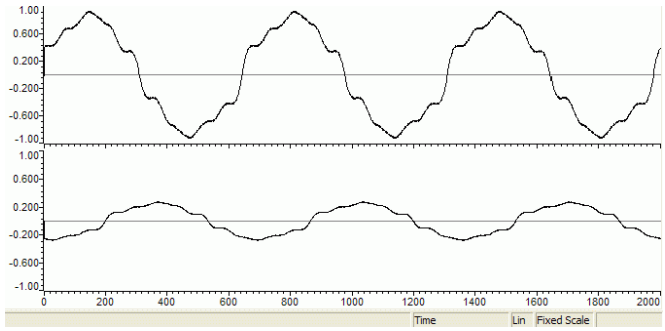

Fig. 13. Line-to-line grid voltages with THD_v=7.5 % and UF_v=68%. Horizontal scale: sample, Ts=25µs. Vertical scale: v_{ab} and v_{bc} in p.u.

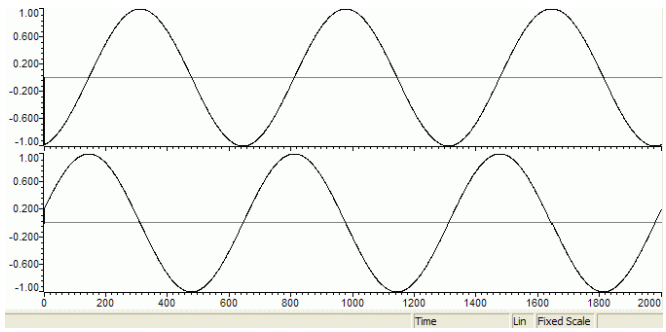

Fig. 14. Synchronization signals obtained using the *NPSF* with the voltages of Fig. 13. Horizontal scale: sample, Ts=25µs. Vertical scale: *sine* and *cosine*.

E. Transient Behavior

Fig. 15 presents experimental results considering transients in grid voltages v_{ab} and v_{bc}. It is possible to see in the Fig. 16 that the synchronization signals do not present significant distortion.

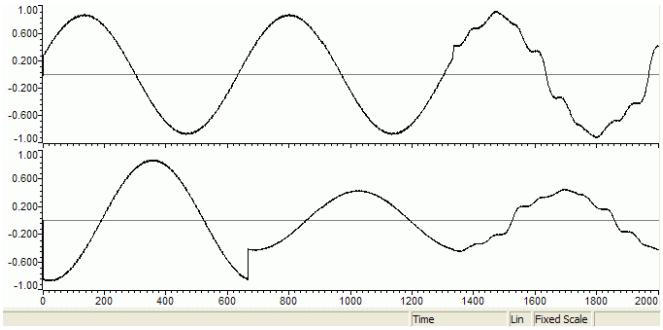

Fig. 15. Line-to-line grid voltages under change of the A to the B and to the D condition. Horizontal scale: sample, Ts=25μs. Vertical scale: v_{ab} and v_{bc} in p.u .

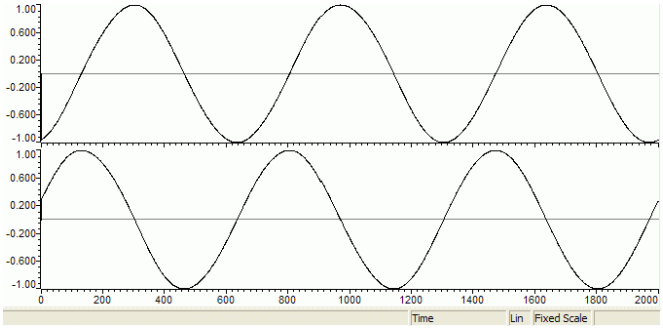

Fig. 16. Synchronization signals under variations in the grid voltages as the Fig. 15. Horizontal scale: sample, Ts=25μs. Vertical scale: *sine* and *cosine*.

Fig. 17 shows the startup transient behavior of the synchronization signals of the *NPSF* method. It is possible to see a fast transient response, where the filter variables have been aleatory selected with a value different of zero at any conditions presented previously.

Fig. 18a shows the transient behavior of the control action of the frequency adaptation algorithm. A frequency step is applied in the grid voltages (58 Hz to 62.5 Hz) at time equal to 0.25 seconds. The settling time is shorter than 1.6 cycles as possible to see that the control action transient. There is a limit cycle in the estimated frequency. This is a result of the truncated parameters matrices which has been stored in the DSP program memory. However, this is of no concern, since it has a high frequency, and can be easily mitigated with an interpolation. Fig. 18b shows the smooth behavior of the *sine* synchronization signal function during the frequency transient.

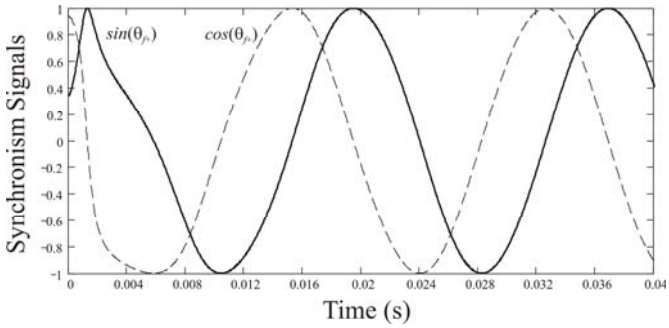

Fig. 17. Transient behavior of the synchronization signals used the *NPSF* method.

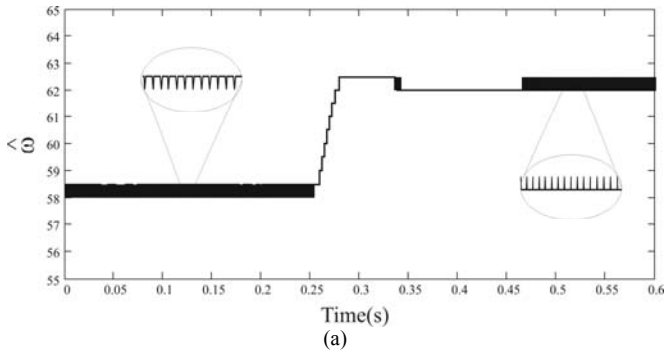

(a)

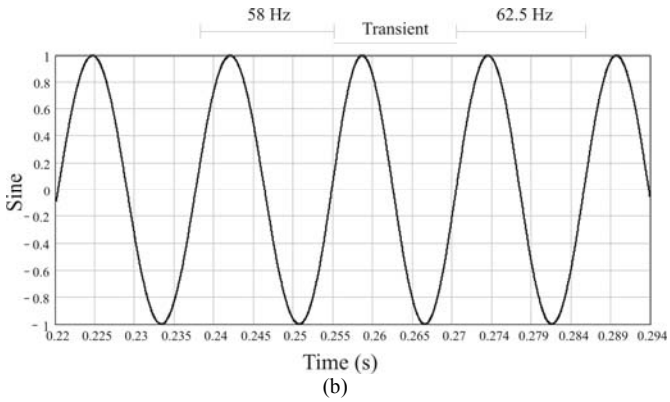

(b)

Fig. 18. *NPSF* method used the frequency adaptation algorithm under frequency step (58Hz to 62.5 Hz). (a) Control action, and (b) Behavior of *sine* synchronization signal.

TABLE I
Open-loop synchronization methods with grid voltage measurement and performance criteria

Criteria / Methods	Harmonic Rejection	Unbalanced Rejection	Adaptability to the frequency variations	Structural Simplicity
MSRF [6, 7]	–	–	Not required	High
LPF-B [9]	Yes	–	–	Middle
SVF [9]	Yes	–	–	Middle
MSVF [9]	Yes	–	Yes	Middle
EKF [9]	Yes	–	Yes	Low
WLSE [17]	–	Yes	Yes	Low
NPSF *	**Yes**	**Yes**	**Yes**	**Middle**

* *Proposed Method*

V. CONCLUSIONS

This paper proposes a new synchronization method to PWM converters connected to the utility. In terms of synchronization signals, it performs better than other *open-loop* methods in the presence of grid voltage unbalance and harmonics, as summarized in Table I. In addition, a frequency adaptation algorithm is developed for applications where large frequency variations are expected, as in weak grids.

Experimental results for synchronization signals when step frequency, unbalanced and harmonics are applied to the grid voltages, confirm the good performance of the proposed method as well as the frequency adaptation algorithm.

In addition, the proposed *NPSF* synchronization method can be easily extended to three-phase four-wire systems.

APPENDIX

A. Unbalance Factor (UF)

Unbalance factor in the voltages can be defined as the maximum deviation from the average of the three-phase voltage, divided by average of the three-phase voltage, as definition in the IEEE Std.1159-1995, that is,

$$UF_v = \left(\frac{\left| V_{frms} - V_{avg} \right|_{\max}}{V_{avg}} \right) 100;$$

B. Total Harmonic Distortion (THD)

Total harmonic distortion in the voltages is defined in the IEEE Std. 519-1992 or IEC 61000-2-2, as follow:

$$THD_V = \left(\sqrt{\sum_{h=2}^{\infty} V_h^2} \Big/ V_1 \right) 100;$$

ACKNOWLEDGEMENT

The authors would like to thank the Mr. Alexandre T. Pereira, Mr. Jorge Massing, and Mr. Felipe Grigoletto for assistance, and the CEEE, CAPES and CNPq for the financial support.

REFERENCES

[1] G.-C. Hsieh and J. C. Hung, "Phase-locked loop techniques – A survey," *IEEE Trans. on Industrial Electronics*, vol. 43, pp. 609-615, Dec. 1996.

[2] S.-J. Lee, J.-K. Kang and S.-K. Sul, "A new phase detecting method for power conversion systems considering distorted conditions in power system," *in Proc. of IAS '99*, pp. 2167-2172, 1999.

[3] D. R. Costa Jr., L.G.B. Rolim and M. Aredes, "Analysis and software implementation of a robust synchronizing circuit PLL circuit," *in Proc. of ISIE '03*, pp. 292-297, 2003.

[4] S. M. Deckmann, F. P. Marafão and M. S. de Pádua, "Single and three-phase digital PLL structures based on instantaneous power theory," *in Proc. of COBEP'03*, pp. 225-230, 2003.

[5] M. Karimi-Ghartemani and M. R. Iravani, "A method for synchronization of power electronic converters in polluted and variable-frequency environments," *IEEE Trans. on Power Systems*, vol. 19, pp. 1263-1270, Aug. 2004.

[6] V. Soares and G. D. Marques, "Active power filter control circuit based on the instantaneous active and reactive current id-iq method," *in Proc. of PESC'97*, pp. 1096-1101, 1997.

[7] G. D. Marques, "A comparison of active power filter control methods in unbalanced and non-sinusoidal conditions," *in Proc. of IECON'98*, pp. 444-449, 1998.

[8] J. L. Duarte, A. V. Zwam, C. Wijnands and A. Vandenput, "Reference frames fit for controlling PWM rectifiers," *IEEE Trans. on Industrial Electronics*, vol. 46, pp. 628-630, Jun. 1999.

[9] J. Svensson, "Synchronization methods for grid-connected voltage source converters," *IEE Proceedings Generation Transmission and Distribution*, vol. 148, pp. 229-235, May 2001.

[10] M. Malinowski and M. P. Kasmierkowski, "Direct power control of three-phase PWM rectifier using space vector modulation- simulation study," *in Proc. of ISIE'02*, pp. 1114-1118, 2002.

[11] S. Hansen, M Malinowski, F Blaabjerg and M. P. Kazmierkowski, "Sensorless control strategies for PWM rectifier," *in Proc. of APEC'00*, pp. 832-838, 2000.

[12] R. M. Kennel, M. Linke and P. Szczupak, "Sensorless control of 4-quadrant-rectifiers for voltage source inverters (VSI)," *in Proc. of PESC'03*, pp. 1057-1062, 2003.

[13] P. Szczupak and R. Kennel, "Sensorless control of PWM rectifiers by distorted supply voltage," *in Proc. of PESC'04*, pp. 203-206, 2004.

[14] M. Cichowlas and M. Kazmierkowski, "Comparison of current control techniques for PWM rectifiers," *in. Proc. ISIE'02*, pp. 1259-1263, 2002.

[15] K. Dai, P. Liu, J. Xiong and J, Chen, "Comparative study on current control, for three-phase SVPWM voltage-source converter in synchronous rotating frame using complex vector method," *in. Proc. of PESC'03*, pp. 695-700, 2003.

[16] M. Malinowski, M. Kazmierkowski and A. M. Trynadlowski, "A comparative study of control techniques for PWM rectifiers in AC adjustable speed drives," *IEEE Trans. on Power Electronics*, vol. 18, pp. 1390-1396, Nov. 2003.

[17] H.-S. Song and K. Nam, "Instantaneous phase-angle estimation algorithm under unbalanced voltage-sag conditions," *IEE Proc. Generation Transmission and Distribution*, vol. 147, pp. 409-415, Nov. 2000.

[18] R. F. Camargo, F. Botterón, M. H. Duarte, J. Marques, H. Pinheiro, "Análise e implementação de retificadores PWM trifásicos com resposta deadbeat utilizando desacoplamento por retroação de estados," *in proc. of CBA '04*, in CD-ROM, 2004.

[19] R. F. Camargo and H. Pinheiro, "Deadbeat decoupled controller by state feedback for three-phase PWM rectifiers and comparative stability analysis," *in. Proc. of INDUSCON'04*, in CD-ROM, 2004.

[20] L. Harnefors and H.P. Nee, "A general algorithm for speed and position estimation of AC motors," *IEEE Trans. on Industrial Electronics*, vol. 47, pp. 77–83, Feb. 2000.

[21] H. Awad, J. Svensson and M. Bollen, "Phase-locked loop for static series compensator," *in. proc. of EPE'03*, in CD-ROM, 2003.

[22] V. Chuvychin, N. Gurov, S. Rubcov and V. Strelkovs, "Problems of power system frequency control during emergency condition," *in proc. of EPE'04*, in CR-ROM, 2004.

[23] G. Maozhong, L. Hankui, G. Hanjun and X. Dianguo, "Active voltage regulator based on novel synchronization method for unbalance and fluctuation compensation," *in Proc. of IECON'02*, pp. 1374 – 1379, 2002.

[24] E. M. Sasso, G. G. Sotelo, A. A. Ferreira, E. H. Watanabe, M. Aredes, P. Barbosa, "Investigação dos modelos de circuitos de sincronismo trifásicos baseados na teoria de potências real e imaginária instantâneas (p-PLL e q-PLL)", *in. Proc. of CBA'02*, in CD-ROM, 2002.

[25] L. C. G. Lopes, R. L. Carletti, P. G. Barbosa, "Implementation of a digital and a dead-beat PLL circuit based on instantaneous power theory with DSP TMS320F243", *in. Proc. of COBEP'03*, in CD-ROM, 2003.

[26] F. P. Marafão, S. M. Deckmann, J. A. Pomílio, R. Q. Machado, "A software-based PLL model: analysis and applications", *in. Proc. of CBA'04*, in CD-ROM, 2004.

[27] R. F. Camargo and H. Pinheiro, "New synchronization method for three-phase four-wire PWM converters under unbalance and harmonics in the grid voltages," *in Proc. of EUROPES'05*, in CD-ROM, 2005.

BIOGRAPHIES

Robinson Figueiredo de Camargo was born in Santa Maria, RS, Brazil, in 1976. He received the B.S. and M. Eng. degrees in electrical engineering from the Federal University of Santa Maria, Santa Maria, Brazil, in 2000 and 2002, respectively.

He is currently working for a doctorate in electrical engineering at the Federal University of Santa Maria. His research interests include digital control techniques of static converters, active power filter, three-phase PWM rectifier and synchronization methods. Mr. Camargo is currently a member of the Brazilian Power Electronics Society (SOBRAEP) and Brazilian Automation Society (SBA).

Humberto Pinheiro was born in Santa Maria, Brazil, in 1960. He received the B.S. degree from the Federal University of Santa Maria, Santa Maria, in 1983, the M. Eng. degree from the Federal University of Santa Catarina, Brazil, in 1987, and the Ph.D. degree from Concordia University, Montreal, Quebec, Canada, in 1999.

He lectured on power electronics at PUC University, Brazil, from 1987 to 1991. He is presently a Professor in the Department of Electronics and Computer Engineering, Federal University of Santa Maria, Brazil. His research interests include control of uninterruptible power supplies and wind turbine systems.